Supporting information

Wearable and Fully-Biocompatible All-in-One Structured "Paper-like" Zinc Ion Battery

Zhipeng Shao[1], Situo Cheng[1], Yaxiong Zhang[1], Hongzhou Guo[1], Xiaosha Cui[1], Zhenheng Sun[1], Yupeng Liu[1], Yin Wu[1], Peng Cui[1], Jiecai Fu[1]*, Qing Su[1] and Erqing Xie[1]*

[1]Key Laboratory for Magnetism and Magnetic Materials of the Ministry of Education, School of Physical Science and Technology, Lanzhou University, Lanzhou 730000, P. R. China

*Corresponding authors

Key Laboratory for Magnetism and Magnetic Materials of the Ministry of Education, School of Physical Science and Technology, Lanzhou University, Lanzhou 730000, P. R. China

E-mail: fujc@lzu.edu.cn (J. Fu); xieeq@lzu.edu.cn (E. Xie).

Energy and power density calculation

The average volumetric power density P_v and energy density (E) were calculated according to following equations (2-3):

$$E = \frac{1}{2} CV^2 \tag{2}$$

$$P_v = E_v / I\Delta t \tag{3}$$

The specific capacity can be calculated *via* the equation (4) and (5) as follows:

GCD curves:

$$C_s = \frac{Q}{V} = I\,\Delta t / V \tag{4}$$

CV curves:

$$C_s = Q/V = S/2vV \tag{5}$$

Where C_s (F cm^{-2}) is the volumetric specific capacitance; Q (C) is the average charge during the charging/discharging process; V (cm^2) is the volume of the all-in-one battery; S (A V) is the integrated area of the CV curve; v (V s^{-1}) is the scan rate; I (A) is the constant discharging current; Δt (s) is the discharging time.

The specific capacitance (C, F cm^{-2}) can be calculated *via* the equation (6) as follows:

$$C = C_s/\Delta V \tag{6}$$

Where ΔV (V) is the potential window.

Structural and Morphological Characterization of the Electrodes

The Phase structures and crystal information of the Zn@CNTs were further investigated by HRTEM, XRD in Figure 2c. The HRTEM shows the interplanar distance of Zn were 0.21 nm, 0.24 nm respectively, which are corresponding to the (101) and (002) planes of hexagonal zinc (JCPDS#87-0713). As shown in insert, all of the diffraction peaks can be well-indexed to hexagonal zinc (JCPDS # 04-0831) in the XRD spectrum. XPS measurement was further adopted to characterize the chemical environment of Zn@CNTs. As is shown in Figure S2 (Support information), the two peaks centered at 1045 and 1021.9 eV in the Zn 2p spectrum are characteristic of Zn 2p1/2 and Zn 2p3/2 in Zn@CNTs.

The XRD spectrum shows the diffraction peaks of MnO_2 nanosheets at 36.9° and 65.4°, which are corresponding to the $(11\bar{1})$ and (020) crystal faces of birnessite-type MnO_2 (JCPDS # 43-1456) in insert. The TEM image reveals that MnO_2 nanosheets were deposited on the surface of the interweaved CNTs (Figure 2g). Figure S3 shows the Raman spectra of the MnO_2@CNTs, Raman band at around 640 cm^{-1} could be observed, which is attributed to the three major Mn-O symmetric stretching vibrations of the [MnO_6] group in MnO_2[1-3]. The XPS spectrum displays chemical composition and electronic structure of MnO_2@CNTs. In the full-scan XPS spectrum (Figure S4a), the presence of elemental Zn, Mn, and O signals can be observed. Figure S4b shows the core-level Mn 2p spectrum, the two peaks centered at 654.5 and 642.7 eV are characteristic of Mn $2p_{1/2}$ and Mn $2p_{3/2}$ in MnO_2@CNTs, which are consistent with typical spin energy separation of 11.8 eV for MnO_2. The oxidation valence of Mn was further evaluated by the core-level O 1s spectrum shown in figure S4c, the three peaks centered at 530.2, 531.5, and 532.6 eV are characteristic of the

tetravalent Mn–O–Mn bonds, hydrated trivalent Mn–OH bonds, and H–O–H bonds. Therefore, the average valence state of Mn can be estimated to be ~3.89[4].

Supplementary figures

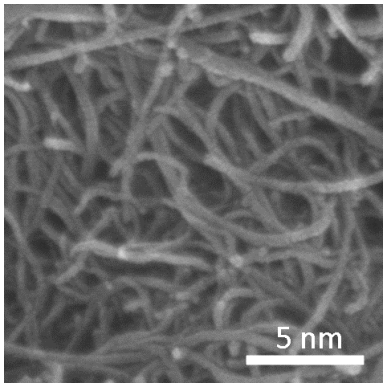

Figure S1. SEM images of the CNTs.

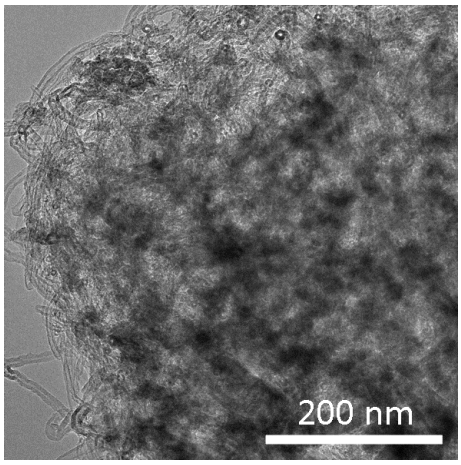

Figure S2. TEM images of the Zn@CNTs.

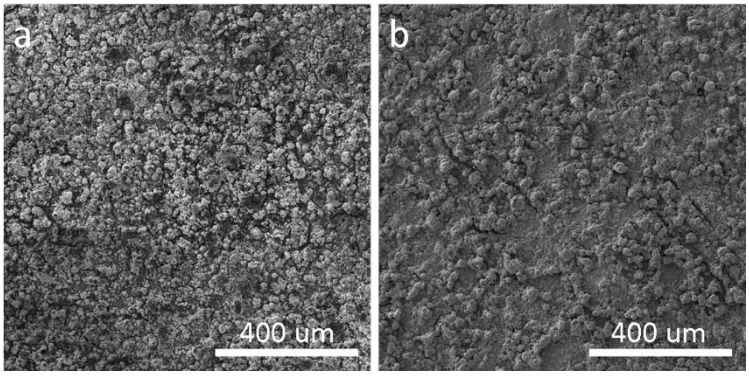

Figure S3. SEM images of the Zn@CNTs (a) and MnO_2@CNTs (b). It can be found that the Zn nanosheets and MnO_2 nanosheets were completely covered on CNT surface.

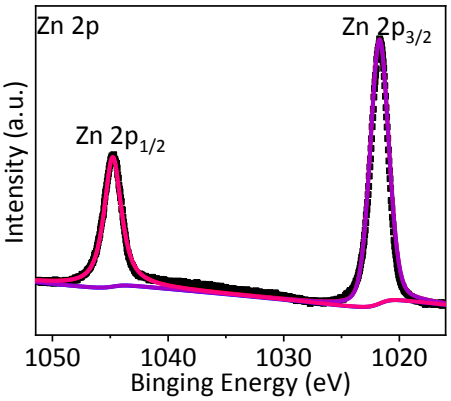

Figure S4. Core-level spectra of Zn 2p elements.

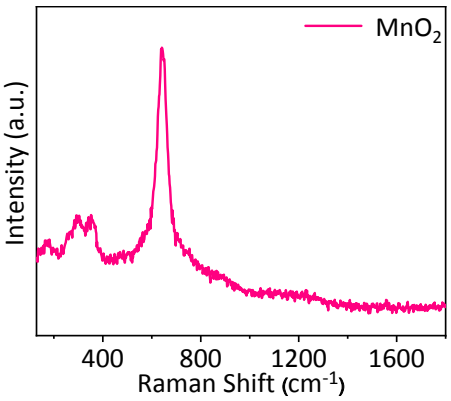

Figure S5. Raman spectra of the MnO_2@CNT.

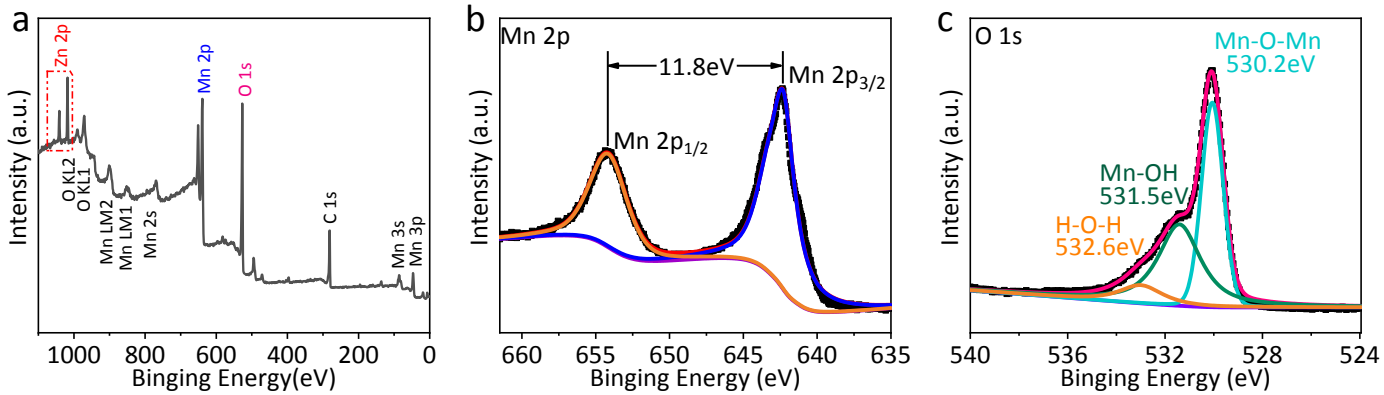

Figure S6. (a) XPS survey spectrum of MnO_2@CNT. (b–c) Core-level spectra of Mn 2p and O 1s elements.

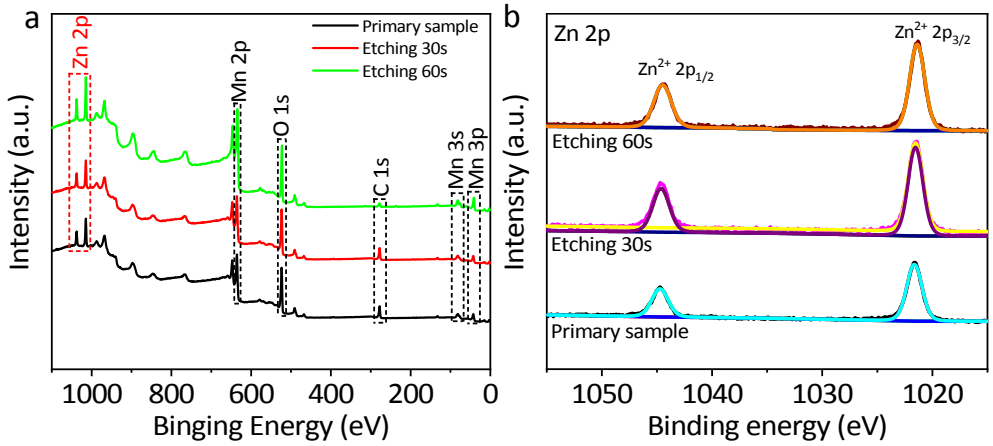

Figure S7. The elemental depth profiles of the MnO_2 pre-intercalated with Zn ions by the Ar ion sputtering depth analysis of XPS: (a) XPS survey spectrum of MnO_2 pre-intercalated with Zn ions. (b) Core-level spectra of Zn 2p elements.

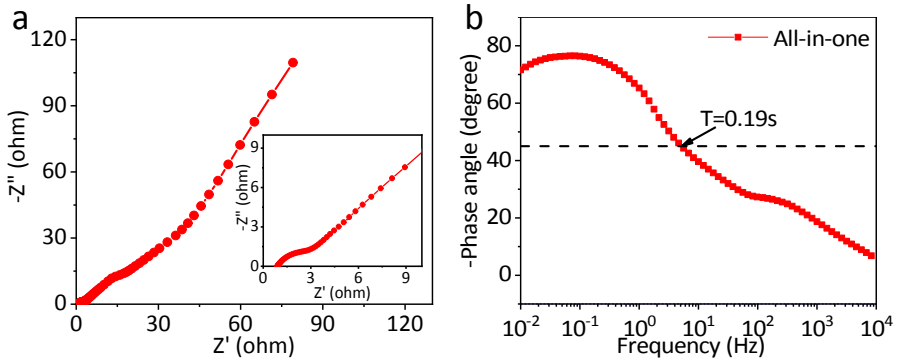

Figure S8. (a) Nyquist plots of the AZMB， the inset shows the magnified Nyquist plots; (b) Bode plots of the AZMB.

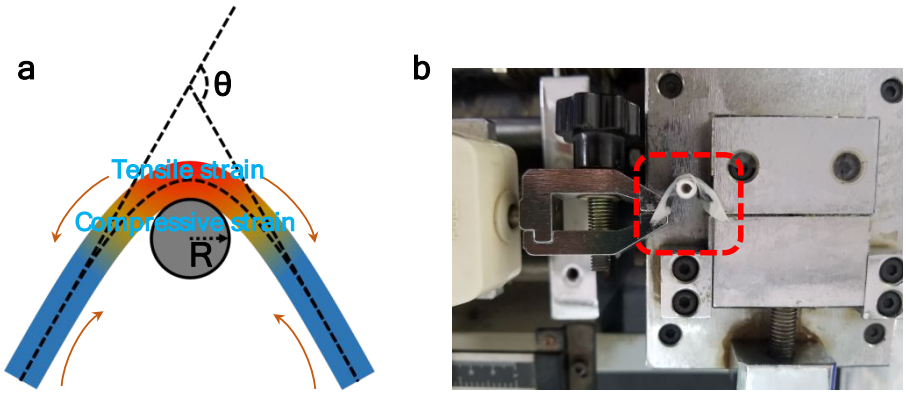

Figure S9. (a) Schematics of structures and the three key parameters (L, θ, and R) that are used to demonstrate the bending state of the AZIB cell; (b) Bending test equipment for AZIB cell.

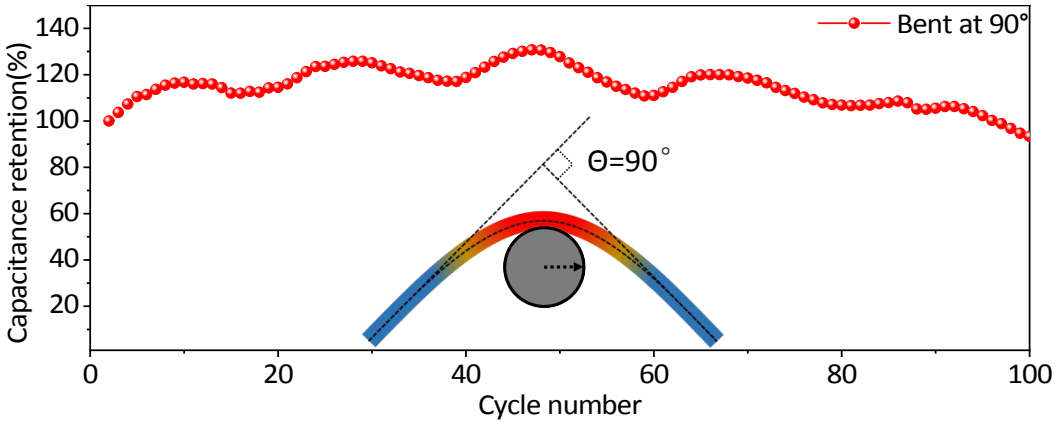

Figure S10. Capacity retention of the AZIB cell bending after 100 cycles at angles of 90°.

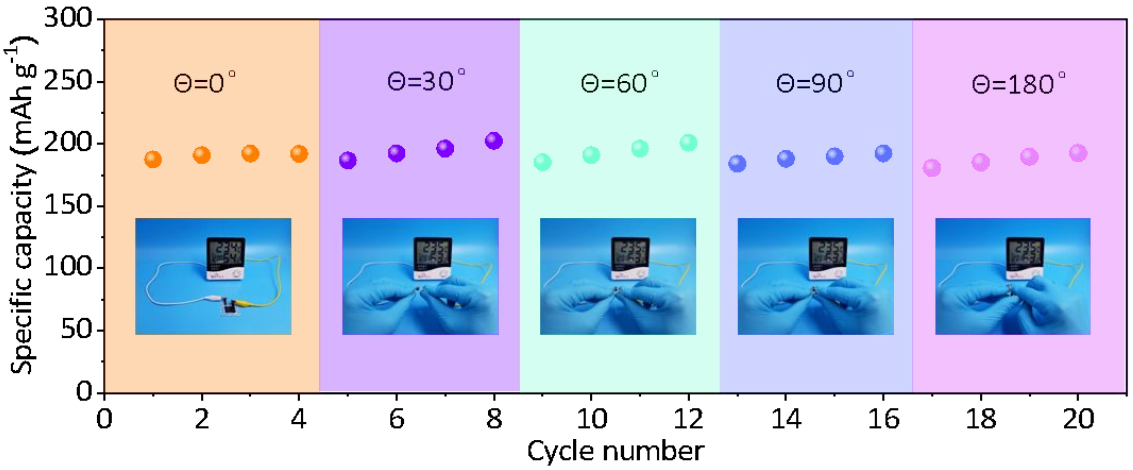

Figure S11. Cycling performance of AZIB cell at different bending angle.

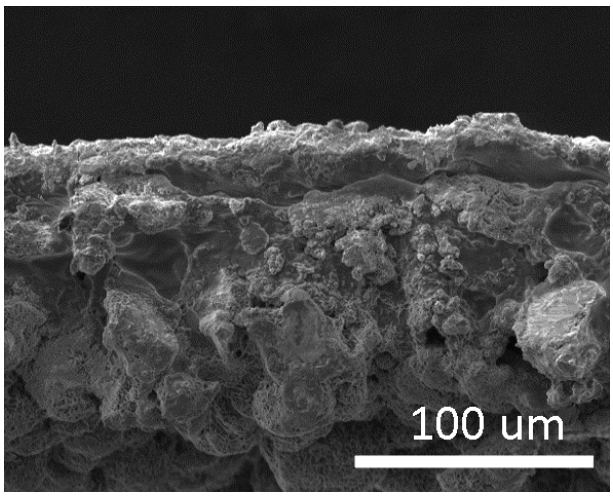

Figure S12. SEM image of the cross-sectional view of the individual battery with gel electrolyte after bending.

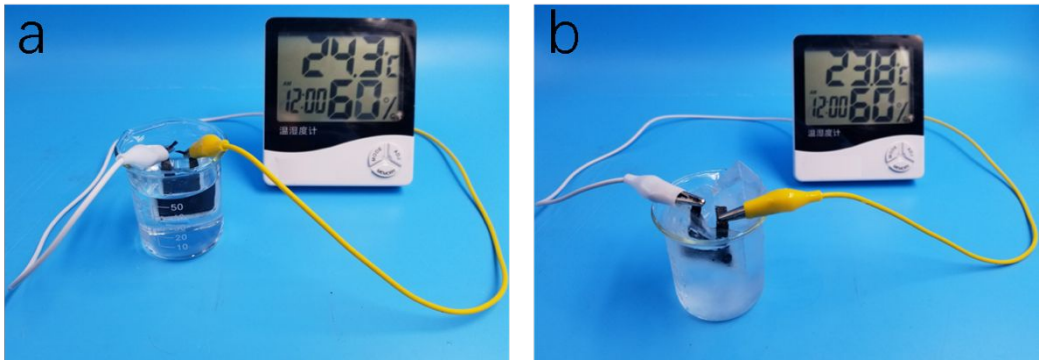

Figure S13. The battery is immersed in water (a) and ice water mixture (b) to power the hygrothermograph.

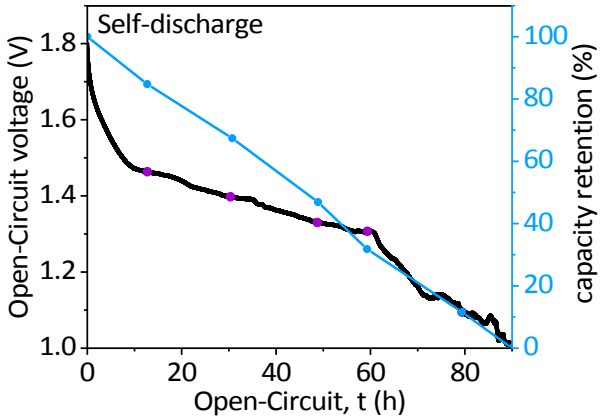

Figure S14. The open-circuit voltage and discharge capacity retention of AZIB cell to evaluate self-discharge rate.

Table S1. Comparison of our AZIB with different flexible ZIBs reported before.

Cathode material	Anode material	Device configuration	Electrolyte	Capacity	Energy density	Power density	Cycling stability	Ref.
MnO_2@CNT	Deposited -Zn@CNT	All-in-one	$ZnCl_2$/ $MnSO_4$/PVA	353.8(0.1 mA cm^{-2})	17.5 mWh cm^{-3} (159 wh kg^{-1})	116.4 mW cm^{-3} (1.06 kw kg^{-1})	98.7% capacity retention after 500 cycles (1A cm^{-2})	This work
GO/PANI	Zn microspheres	All-in-one	PVA-$Zn(SO_3CF_3)_2$	175.5 mAh g^{-1} (0.1 A g^{-1})	-	-	94.6% capacity retention after 500 cycles (1A g^{-1})	5
Air	$Ga_{68.5}In_{21.5}Sn_{10}$	All-in-one	NaOH-ethanol	1.27 mAh cm^{-2} (0.5 mA cm^{-2})	1.52mWh cm^{-2}	2.05 mW cm^{-2}	-	6

PANI@CNT	Zn foil	All-in-One	PVA/Zn $(CF_3SO_3)_2$ hydrogel	123 mAh g^{-1} (0.1A g^{-1})		5.089 Mw kg^{-1}-	97.1% capacity retention after 500 cycles (1A g^{-1})	7
MnO_2@PEDOT@CC	Deposited-Zn@CC	Sandwich structure	$ZnCl_2$/$MnSO_4$/PVA gel	282.4 (0.7 A g^{-1})	504.9 Wh kg^{-1}	8.6 kW kg^{-1}	77.7% capacity retention after 300 cycles	8
MnO_2@the CNT paper	Deposited-Zn@CNT paper	Sandwich structure	$ZnSO_4$/$MnSO_4$/gelatin-g-PAM gel	306	6.18 mW h cm^{-2}	148.2 mW cm^{-2}	97% capacity retention after 1000 cycles (2772 mA g^{-1})	9
$NaV_3O_8 \cdot 1.5H_2O$@the steel meshes	Zn foil	Sandwich structure	Na_2SO_4/$ZnSO_4$/gelatin gel	160 (0.5 A g^{-1})	144 Wh kg^{-1}	–	77% capacity retention after 100 cycles (0.5 A g^{-1})	10
MnO_2/rGO@CC	Deposited-Zn@CC	Sandwich structure	$ZnSO_4$/$MnSO_4$	332.2 (0.3 A g^{-1})	456.2 Wh kg^{-1}	7.9 kW kg^{-1}	96% capacity retention after 500 cycles (6A g^{-1})	11
MnO_2@CNT film	Zn foil	Sandwich structure	$ZnSO_4$/$MnSO_4$/xanthan gel	260 (1C)	364 Wh kg^{-1}	2.5 kW kg^{-1}	90% capacity retention after 330 cycles(1C)	12
Polyaniline@ carbon felts	Zn foil	Sandwich structure	$Zn(CF_3SO_3)_2$/PVA gel	109 (0.5 A g^{-1})	–	–	91.7% capacity retentions after 200 cycles	13
	Zn wire	Cable-type		106 (0.5 A g^{-1})	–	–	91.5% capacity retentions after 200 cycles	
MnO_2@CNT fiber	Zn wire	Cable-type	$Zn(CF_3SO_3)_2$/PVA gel	290 (0.1 A g^{-1})	360 Wh kg^{-1}	100 W Kg^{-1}	75% capacity retention after 300 cycles	3
MnO_2@PPy @ stainless steel	Deposited-Zn@nitinol wire	Cable-type	$ZnSO_4$/$MnSO_4$/gelatin–borax gel	135.2(1C)	–	–	87% capacity retention after 500 cycles	14
MnO_2@CNT yarn	Deposited-Zn@CNT yarn	Double-helix cable-type	$ZnSO_4$/$MnSO_4$/PAM gel	302.1	53.8 mWh cm^{-3}	–	98.5% capacity retention after	15

MnO_2@A4-type paper	Zn foil	Sandwich structure	$ZnSO_4$	285 (0.05 mA cm^{-2})	–	–	500 cycles 64% capacity retention over 40 cycles	[16]
ZnHCF@MnO_2@Ni foil	Zn foil	Sandwich structure	$ZnSO_4$/PVA gel	89 (100 mA g^{-1})	149 Wh kg^{-1}	167 W kg^{-1}	71% capacity retention over 500 cycles(400 mA g^{-1})	[17]

REFERENCES

(1) Ma, S. B.; Ahn, K. Y.; Lee, E. S.; Oh, K. H.; Kim, K. B. Synthesis and Characterization of Manganese Dioxide Spontaneously Coated on Carbon Nanotubes. *Carbon* **2007,** *45* (2), 375-382.

(2) Buciuman, F.; Patcas, F.; Craciun, R.; Zahn, D. R. T. Vibrational Spectroscopy of Bulk and Supported Manganese Oxides. *Phys. Chem. Chem. Phys.* **1999,** *1* (1), 185-190.

(3) Wang, K.; Zhang, X.; Han, J.; Zhang, X.; Sun, X.; Li, C.; Liu, W.; Li, Q.; Ma, Y. High-Performance Cable-Type Flexible Rechargeable Zn Battery Based on MnO_2@CNT Fiber Microelectrode. *ACS Appl. Mater. Interfaces* **2018,** *10* (29), 24573-24582.

(4) Toupin, M.; Brousse, T.; Bélanger, D. Charge Storage Mechanism of MnO_2 Electrode Used in Aqueous Electrochemical Capacitor. *Chem. Mater.* **2004,** *16* (16), 3184-3190.

(5) Zhang, Y.; Wang, Q.; Bi, S.; Yao, M.; Niu, Z. Flexible All-in-One Zinc-Ion Batteries. *Nanoscale* **2019,** *11* (38), 17630-17636.

(6) Wang, Y.; Wang, X.; Xue, M.; Li, Q.; Zhang, Y.; Liu, D.; Liu, J.; Rao, W. All-in-One ENERGISER Design: Smart Liquid Metal-Air Battery. *Chem. Eng. J.* **2021,** *409*, 128160.

(7) Huang, S.; Wan, F.; Bi, S.; Zhu, J.; Niu, Z.; Chen, J. A Self-Healing Integrated All-in-One Zinc-Ion Battery. *Angew Chem. Int. Ed.* **2019,** *58* (13), 4313-4317.

(8) Zeng, Y.; Zhang, X.; Meng, Y.; Yu, M.; Yi, J.; Wu, Y.; Lu, X.; Tong, Y. Achieving Ultrahigh Energy

Density and Long Durability in a Flexible Rechargeable Quasi-Solid-State Zn–MnO_2 Battery. *Adv. Mater.* **2017,** *29* (26), 1700274.

(9) Li, H.; Han, C.; Huang, Y.; Huang, Y.; Zhu, M.; Pei, Z.; Xue, Q.; Wang, Z.; Liu, Z.; Tang, Z. An Extremely Safe and Wearable Solid-State Zinc Ion Battery Based on a Hierarchical Structured Polymer Electrolyte. *Energy Environ. Sci.* **2018,** *11* (4), 941-951.

(10) Wan, F.; Zhang, L.; Dai, X.; Wang, X.; Niu, Z.; Chen, J. Aqueous Rechargeable Zinc/Sodium Vanadate Batteries with Enhanced Performance from Simultaneous Insertion of Dual Carriers. *Nat. Commun.* **2018,** *9* (1), 1656.

(11) Huang, Y.; Liu, J.; Huang, Q.; Zheng, Z.; Hiralal, P.; Zheng, F.; Ozgit, D.; Su, S.; Chen, S.; Tan, P.-H.; Zhang, S.; Zhou, H. Flexible High Energy Density Zinc-Ion Batteries Enabled by Binder-Free MnO_2/Reduced Graphene Oxide Electrode. *npj Flexible Electronics* **2018,** *2* (1).

(12) Zhang, S.; Yu, N.; Zeng, S.; Zhou, S.; Chen, M.; Di, J.; Li, Q. An Adaptive and Stable Bio-Electrolyte for Rechargeable Zn-Ion Batteries. *J. Mater. Chem. A* **2018,** *6*, 12237-12243.

(13) Wan, F.; Zhang, L.; Wang, X.; Bi, S.; Niu, Z.; Chen, J. An Aqueous Rechargeable Zinc-Organic Battery with Hybrid Mechanism. *Adv. Funct. Mater.* **2018,** *28* (45), 1804975.1-1804975.8.

(14) Wang, Z.; Ruan, Z.; Liu, Z.; Wang, Y.; Tang, Z.; Li, H.; Zhu, M.; Hung, T. F.; Liu, J.; Shi, Z.; Zhi, C. A Flexible Rechargeable Zinc-Ion Wire-Shaped Battery with Shape Memory Function. *J. Mater. Chem. A* **2018,** *6* (18), 8549-8557.

(15) Li, H.; Liu, Z.; Liang, G.; Huang, Y.; Huang, Y.; Zhu, M.; Pei, Z.; Xue, Q.; Tang, Z.; Wang, Y. Waterproof and Tailorable Elastic Rechargeable Yarn Zinc Ion Batteries by a Cross-Linked Polyacrylamide Electrolyte. *ACS Nano* **2018,** *12* (4), 3140-3148.

(16) Alfaruqi, M. H.; Mathew, V.; Gim, J.; Kim, S.; Kim, J. Electrochemically Induced Structural Transformation in a γ-MnO_2 Cathode of a High Capacity Zinc-Ion Battery System. *Chem. Mater.* **2015,** *27*

(10), 3609-3620.

(17) Lu, K.; Song, B.; Zhang, Y.; Ma, H.; Zhang, J. Encapsulation of Zinc Hexacyanoferrate Nanocubes with Manganese Oxide Nanosheets for High-Performance Rechargeable Zinc Ion Batteries. *J. Mater. Chem. A* **2017,** *5* (45), 23628-23633.